Journal of Molecular Liquids, 34 (1987) 285–306
Elsevier Science Publishers B.V., Amsterdam – Printed in The Netherlands

THE DYNAMICS OF LIQUID WATER: SIMULATION AND SUBMILLIMETER SPECTROSCOPY

G.J. Evans[1], M.W. Evans[2], P. Minguzzi[3], G. Salvetti[4], C.J. Reid[3] and J.K. Vij[5]

1. Dept. of Chemistry, University College of Wales, Aberystwyth, SY23 1NE, Wales (UK).
2. Dept. of Physics, University College of Swansea, Singleton Park, Swansea, SA2, 8PP, Wales (UK). *
3. Dipartimento di Fisica, Univ. di Pisa, Piazza Torricelli, 56100, Pisa, Italy
4. Istituto di Fisica Atomice e Moleculare del C.N.R., Via del Giardino, Pisa, Italy.
5. Dept. of Microelectronics and Electrical Engineering, Trinity College, Dublin 2, Ireland.

* Current Address: IBM, Dept. 48B/428, Neighborhood Rd. Kingston,NY 12401, USA

(Received 22 September 1986)

ABSTRACT

A combination of classical molecular dynamics computer simulation and submillimeter laser and interferometric spectroscopy is used to investigate the dynamical and structural properties of liquid water at 300 K, ρ = 0.997 gm cm^{-3}. A new approach to the empirical pair potential, based on the ST2 of Raman and Stillinger has been used to match the low frequency part of the submillimeter spectrum and to generate a range of auto and cross correlation functions. The results from this new atom-atom potential have been compared with those from the work of Stillinger and Rahman and Clementi et al. Broad agreement was obtained and the new potential used to investigate by computer simulation the statistical interdependence of the water molecule's rotation and translation in liquid water at 300 K. This investigation has resulted in the detection of a.c.f.'s of the classical Coriolis, centripetal, and "non uniform" accelerations of the water molecule, together with some of the numerous cross correlations suggested by the rotating frame theory of Langevin diffusion.

INTRODUCTION

There are numerous empirical representations of the potential energy of interaction between two water molecules. These have been evaluated carefully

0167-7322/87/$03.50

by Morse and Rice [1] in a recent paper which shows that none is entirely satisfactory. The theoretical description of molecular dynamics in liquid water, and related, for example spectral, properties, must therefore wait for progress in our fundamental understanding of the intermolecular potential. The developments over a decade of intensive computer based research on ice and water can be gauged by reference to two key papers, one by Stillinger and Rahman [2] in 1974 and the other by Clementi et al. [3] which appeared in 1985. Both papers use the technique of molecular dynamics computer simulation to investigate the classical equations of motion for water and to calculate a variety of thermodynamic and structural properties using the methods of non-equilibrium statistical mechanics. Clementi et al. [3] were able to use ab initio calculations of the inter-molecular potential for water and to incorporate three and four body interaction terms into Monte Carlo and Molecular Dynamics simulations. The stage is therefore set for the first fully self consistent theoretical calculation [4] of the molecular dynamical properties of water and ice. The last remaining difficulty seems to be the continued reliance on the classical equations of motion. Lie and Clementi [5] have introduced already an intermolecular potential based on ab initio methods, and have used this directly in their simulations.

The progress made in understanding the nature of the intermolecular potential for water has been paralleled by an increase in the number of ways in which auto-correlation functions (a.c.f.'s) and cross-correlation functions (c.c.f.'s) can be used to look at the details of the molecular dynamics [6-10]. The c.f.'s can also be Fourier transformed into frequency dependent spectra of several different kinds [9,10] using computer simulation to interpret self consistently the whole range of data. The vast aqueous literature makes this an awesome task for ice and water, but inroads in this direction are being made [11]. This paper uses a combination of classical molecular dynamics simulation and submillimeter laser and broad band spectroscopy [10] to estimate how far the classical approach succeeds in reproducing the picosecond and femtosecond dynamics of liquid water at room temperature. Section I describes the empirical pair potential and computer simulation algorithm; Section II the spectroscopic methods; Section III the experimental spectral results and Section IV the numerical results from the simulation of the atom atom pair distribution functions together with a number of single molecule a.c.f.'s and c.c.f's in the laboratory frame (x,y,z) and in the moving frame (1,2,3) of the principal molecular moments of inertia. Finally in section V we suggest ways of increasing our understanding

of the dynamical properties of liquid water by comparing the results for c.c.f's with predictions from group theory.

SECTION I: THE EMPIRICAL PAIR POTENTIAL AND COMPUTER SIMULATION ALGORITHM

This is a modified ST2 potential which includes atom-atom terms centred both on the oxygen and hydrogen atoms. This method eliminates automatically the need to use the switching function devised by Stillinger and Rahman [2]. The empirical pair potential is then described as follows:

$$\varepsilon/k(O\text{-}O) = 58.4 \text{ K}; \quad \sigma(O\text{-}O) = 2.8 \text{ Å};$$

$$\varepsilon/k(H\text{-}H) = 21.1 \text{ K}; \quad \sigma(H\text{-}H) = 2.25 \text{ Å};$$

$$\varepsilon/k(O\text{-}H) = \left| \frac{\varepsilon}{k}(O\text{-}O) \frac{\varepsilon}{k}(H\text{-}H) \right|^{\frac{1}{2}}$$

$$\sigma(O\text{-}H) = \tfrac{1}{2}(\sigma(O\text{-}O) + \sigma(H\text{-}H));$$

where $\frac{\varepsilon}{k}$ and σ are the usual atom-atom Lennard Jones parameters. In addition the original tetrahedral arrangement of charges in the ST2 potential was used unchanged, together with the original ST2 geometry (fig. (1)). The atom-atom parameters quoted above were based closely on independent experimental estimates. [12]

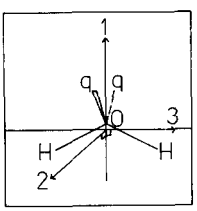

Fig. 1. Illustration of the ST2 potential of water, and definition of frame (1,2,3) of the text.

With a time step of 5.0×10^{-16} sec (0.5 femtosecond) a sample of only 108 molecules, no Ewald corrections [13], and simple cubic periodic boundary conditions, the total mean configurational energy at 300 K; $\rho = 0.997$ gm cm^{-3}; molar volume = 18.07 cm^3/mole; was for a typical segment of about 1000 time steps - 35.5 kJ/mole; the mean pressure - 137 ± $(1.15 \times 10^6)^{\frac{1}{2}}$ bar. This compares well with a value of - 34.3 kJ/mole at 314 K obtained by Stillinger and Rahman [2], also in the absence of Ewald corrections. For two body

interactions the use of Ewald sums by Clementi et al. [3] reduced this value to - 38.6 kJ $mole^{-1}$ and the inclusion of three and four body terms brought this closer to the experimental result [3] of - 41.0kJ/mole.

These results, by all three groups, were obtained by integrating the classical equations of motion, and further improvements will be obtainable by incorporating quantum effects. The most obvious of these is bond vibration on a femtosecond and sub-femtosecond scale, both inter and intra molecular.

The algorithm used in this paper treats the ST2 water molecule as a rigid body obeying the classical laws of dynamics. The equations of motion were integrated numerically in two stages, [14] the total torque on each molecule was first computed from the atom atom and charge charge forces and the angular momentum in frame (1,2,3) then computed by integration over the four previous time steps. The translational equation of motion was integrated numerically with Verlet's algorithm and the cut off criterion applied with respect to the intermolecular centre of mass separation. The total energy was observed to be constant to within a few parts in a thousand. Long range corrections were applied to the virial sum and to the total configurational energy for Lennard Jones terms only, because they diverge for charge charge terms. [13] The range of a.c.f.'s and c.c.f's illustrated in Section III were evaluated with running time averages over two or more segments of 1000 time steps each, and atom-atom pair distribution functions evaluated for oxygen oxygen; hydrogen-hydrogen; and oxygen hydrogen interactions over about 5000 consecutive time steps at equilibrium. Finally the rotational velocity a.c.f. was Fourier transformed into the far infra red spectrum using the Cooley Tukey Fast Fourier Transform. [15]

SECTION 2: EXPERIMENTAL METHODS

Submillimeter Laser Spectroscopy

This was carried out at the Physics Department, University of Pisa. The radiation source was an Apollo Instruments submillimeter laser system, [16] composed of a continuous wave CO_2 laser and a far infra-red laser. The system was modified to improve its passive stability, and was operated free running with active stabilisation circuits disconnected. The output power of the CO_2 laser is continuously monitored by a separate pyrroelectric detector, which is useful to control the operation of the pump laser. The whole experiment was isolated on a vibration free table. A few spot frequencies of monochromatic radiation were obtained by pumping methanol vapour and one by pumping methyl

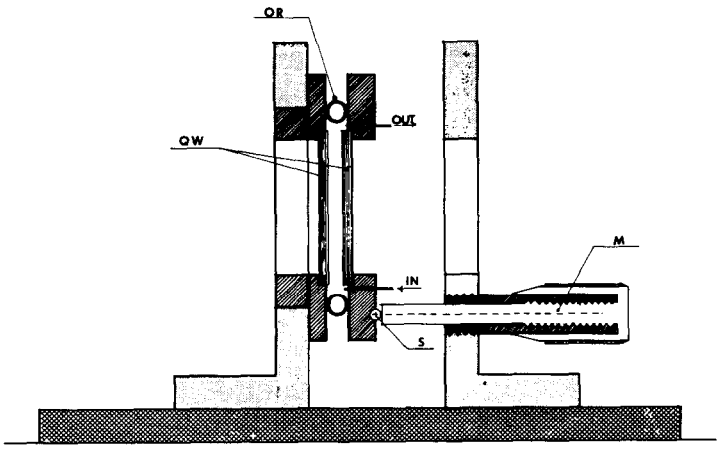

Fig. 2. The experimental cell. QW - quartz windows; M - one of the three micrometers, arranged equilaterally; S - stainless steel sphere; IN/OUT the needles through which the liquid is introduced. OR - "O" Ring.

iodide vapour at 22 cm^{-1}. The wavenumber range covered is from 22 cm^{-1} to 142 cm^{-1}. The power absorption coefficient of liquid water at these frequencies was obtained with the use of a sample cell specially designed and constructed for this experiment at I.F.A.M. (Pisa). Its main features are illustrated in fig. (2). The windows are crystalline quartz 40 mm in diameter and are checked for parallelism with the help of an auxilliary He/Ne laser. The liquid is injected through a needle placed at the bottom of the cell, whereas a second needle at the top prevents the formation of bubbles between the windows. The pathlength d can be set by three micrometers arranged equilaterally with one micron resolution. The absolute accuracy in the measurement of d is estimated conservatively at 5 μm.

Most measurements were taken with a double beam configuration, both the incident, I_o, and transmitted, I, power can be observed by a single Golay detector. By repeated switching of the laser beam between the two light paths many measurements of the ratio I_o/I can be accumulated in a short time. The pump laser is either mechanically chopped or used in the "long pulse" mode (for weaker lines) and a lock-in amplifier is used to detect the Golay signal. The power absorption ratio I_o/I was plotted on a semi-logarithmic scale as a function of the cell length d for immediate visual inspection of possible incorrect data, and for a preliminary estimate of the power absorption coefficient from the slope of the straight line. The runs judged satisfactory

were later analysed by a weighted least squares computer programme to estimate the parameters of the exponential decay and their covariance matrix.

The accuracy of the power absorption coefficient ranges from better than 2% (at 95% confidence level) for strong, stable, lines to about 12% for weak lines. A set of measurements taken for mixtures of methanol and water at different concentrations and the results are summarised in table 1. The experimental data for pure water are also presented in fig. (3) as described in detail below. All measurements were taken at room temperature (301 K), the purity of the methanol being 99.9% and the water being 99.996% pure and double distilled. A few, less accurate, measurements were taken at Bangor before the apparatus was transferred to Pisa and they can be identified by the larger uncertainties in table (1) and fig. (3).

TABLE 1

Power Absorption Coefficients (neper cm^{-1}) at Different Submillimeter Frequencies

	Frequencies (cm^{-1})						
Solution	22.363	38.772	42.963	58.629	61.337	84.151	106.30
H_2O	179(6)	280(30)	260(10)	307(12)	325(35)	400(6)	525(20)
0.125 m.f. CH_3OH/H_2O				240(5)		320(7)	455(50)
0.250 m.f. CH_3OH/H_2O	101(8)			203(8)		291(5)	390(20)
0.500 m.f. CH_3OH/H_2O	84(6)			178(5)		248(10)	330(15)
0.750 m.f. CH_3OH/H_2O	74(4)			170(4)		224(4)	300(15)
CH_3OH	80(4)			175(8)		205(5)	280(20)

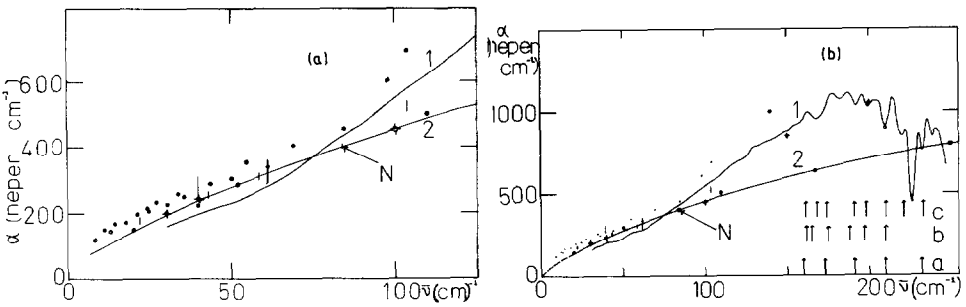

Fig.3. Comparison of our, and other, submillimeter laser points for water (see appendix) with the direct Fourier transform (_____) of $\langle \dot{\underset{\sim}{\mu}}(t).\dot{\underset{\sim}{\mu}}(o)\rangle$ from the computer simulation. The computer simulation result is normalised to the laser point at 84 cm^{-1}.
Ordinate power absorption ($\alpha(\bar{\nu})$) in neper cm^{-1}; abscissawave number (cm^{-1})

BROAD BAND INTERFEROMETRIC SPECTROSCOPY [10]

These measurements were carried out on liquid water by an absorption technique using a Grubb Parsons/N.P.L. Fourier transform spectrometer in the laboratory of G.J. Evans at Aberystwyth. A VC 01 variable path length liquid cell was used to define the path length as accurately as possible.

SECTION 3: EXPERIMENTAL RESULTS

The submillimeter absorption of liquid water is very intense and its accurate measurement is difficult. In fig. (3) laser and interferometric data from a number of sources are collected [17-22] and are plotted with the results of this investigation. The laser points of this work (table 1)) are plotted as bars, the length of each bar estimates the statistical uncertainty in the power absorption at each frequency. A number of additional laser points are shown in fig. (3a). The most detailed results are those of Simpson et al. [18] ( ). These authors claim a statistical uncertainty of about 2%. Some additional laser points are available from the Mainz group and are plotted as . The broad band interferometric data of this work, obtained by G.J. Evans, are plotted as curve 1 of fig. (3(a)). Finally some points obtained recently by Hasted et al. [19] using dispersive broad band interferometry are included as the points fig. (3(a)). The results from the computer simulation have been normalised in intensity to our laser points at 84.151 cm^{-1} because

three of our measurements, two by Dr. Minguzzi and one by Dr. Reid, happened to produce the same value at this frequency of 400 neper cm^{-1}, albeit with varying statistical uncertainty. This point is marked N in fig. (3a) with the statistical uncertainty of table (1) marked on the figure.

The curve marked 2 in fig. (3a) is merely a line drawn through the relatively widely spaced points of fig. (4) and it should be clear therefore that the computer simulation lacks sufficient resolution to reveal anything about the reality or otherwise of the fluctuations clearly visible in the data of Simpson et al. [18] If we accept their estimate of a 2% uncertainty in their data due to statistical fluctuation, and if we neglect for the moment the possibility of systematic uncertainty, then their data will mean that the power absorption coefficient of water in the range illustrated in fig. (3a) is richly structured with peaks. However this conclusion is not supported by the other laser points in fig. (3a) and the broad band data at 2 cm^{-1} resolution shows no structure in this region. Curve 1 of fig. (3a) is a line drawn through these interferometric points. It is interesting to note that the laser points obtained by Simpson et al. [18] are systematically above these from the Apollo laser system, and from the Fabry Perrot system at Mainz. [21] Several of these points fall almost exactly on the curve 2 obtained by computer simulation from the rotational velocity a.c.f. This is probably fortuitous, but indicates that quantum effects up to 50 cm^{-1} are relatively less effective on the power absorption than at higher frequencies. There is a definite change of slope, indicated by the interferometer and laser at about 80 cm^{-1}, although there is substantial and increasing scatter among various experimental

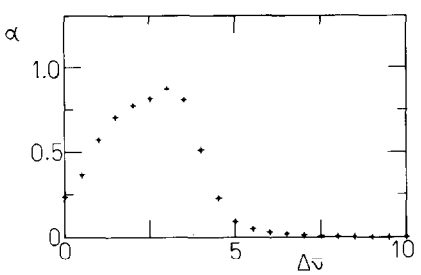

Fig. 4. Digital Fourier transform of $\langle \dot{\underset{\sim}{\mu}}(t).\dot{\underset{\sim}{\mu}}(o) \rangle$ from the simulation. The curve of fig. (3) is estimated by extrapolation, taking into account the finite value at zero frequency in fig. (4).

Ordinate Power absorption in arbitrary units.

Abscissa $\Delta\bar{\nu} = 500/6$ cm^{-1}.

sources at about 100 cm^{-1}. This change of slope is revealed more clearly in fig. (3b) and is not followed by the simple Fourier transform from our classical simulation. This may be an indication of several different phenomena, two of which could be i) quantum effects, such as intra or inter molecular normal mode vibration; [17] ii) inter molecular cross correlations.

Fig. (3b) shows the influence of additional experimental features in the region around 200 cm^{-1} reported by Stanevich and Yaroslavskii [17] and confirmed by G.J. Evans. [20,22] The former used a grating spectrometer and attributed the features to normal mode vibration of water multimers. These frequencies are the arrows marked a in the figure. The frequencies marked b and c were obtained by G.J. Evans [20,22] using respectively a Grubb Parsons/N.P.L. "Cube" interferometer with polymeric windows in the absorption cell and a Nicolet Instruments modern generation Fourier transform interferometer with independent optics, software and cell configuration. Curve 1 of fig. (3b) is the result obtained by Evans [20,22] at 2 cm^{-1} resolution, using a third independent cell configuration with quartz windows. The points marked are from the computer simulation of this work, the curve 2 is hand drawn through these, using the additional information that the power absorption coefficient is zero at zero frequency. The points are those of Simpson et al. [18] as in fig. (3a), the bars are the laser results of this work; the points were obtained on the Mainz laser; [21] and the points are taken from the dispersive interferometric work of Hasted et al. [19] The figure shows clearly that the results from the computer simulation do not reproduce the experimental data after about 100 cm^{-1} in slope or intensity. The resolution of the computer simulation is insufficient to say anything about the reality or otherwise of the peaks in the 200 cm^{-1} region. Fig. (4) shows furthermore that the classical computer simulation for water fails completely at about 600 cm^{-1} in that the continuum absorption known to characterise water in the mid infra-red is missing completely from the Fourier transform of the a.c.f. of the rotational velocity illustrated on various scales in fig. (3). A considerable amount of further work is therefore needed to follow the molecular dynamics of liquid water at these frequencies. This requires consideration of the full N body problem in Schrödinger's equation, taking full account of vibration, [5] rotation, and translation, together with many body effects [3] in the ab initio pair potential.

The classical far infra-red absorption in pure liquid methanol has been simulated elsewhere, [23] and in this paper we confine the analysis of the water/methanol data to noting that the effect of dilution by water seems to have

an approximately linear effect at these frequencies. There is a sign of a peak or a shoulder in the pure liquid methanol power absorption at about 60 cm^{-1} and this will be subject of future computer simulations. We note that the _____ experimental far infra-red power absorption of pure liquid water is well known [11] to peak at about 700 cm^{-1}. The dilution of water in organic solvents has shown [24] that this peak fall to about 200 cm^{-1} when the intermolecular H-bonding is removed and replaced by water/CCl_4; water/benzene; and water/cyclohexane interactions. There is no hope of producing the complete experimental broad-band of water, plus superimposed peak structure with the classical equations of motion as used in nearly all contemporary computer simulation.

In the Fourier transform of the rotational velocity a.c.f.

$$c(t) = \langle \dot{\underset{\sim}{\mu}}(t) \cdot \dot{\underset{\sim}{\mu}}(o) \rangle \; / \; \langle \dot{\mu}^2 \; (o) \rangle \qquad (1)$$

it is however just possible to discern, (fig. (4)), a shoulder at about 250 cm^{-1}, followed by the "classical peak" at about 500 cm^{-1}. The resolution is however insufficient to say more about the observed spectrum. A fuller, theoretical, treatment would involve the complete, multi-molecular, c.c.f.

$$C_1(t) = \langle \sum_i^N (\dot{\underset{\sim}{\mu}}_i(o) \; . \; \sum_i^N \dot{\underset{\sim}{\mu}}_i(t)) \rangle \qquad (2)$$

which in turn needs a bigger sample than the 108 molecules used in this work for C(t). It would also be necessary to work with an ab initio pair potential, [5] and to incorporate vibrational, and multi-body effects. It might be significant that the shoulder in the classical simulation of fig. (4) is roughly at the same frequency as the far infra-red water peak in dilute solutions [24] in organic solvents such as benzene, cyclohexane, or carbon tetrachloride. *This is the intrinsic torsional oscillatory peak due to the* liberation of the single water molecule when freed from hydrogen bonding. The *two features in fig. (4) are due to the average resultant torsional oscillatory* motion of each water molecule in the presence of hydrogen bonding as modelled by our modified ST2 potential.

SECTION 4: PAIR DISTRIBUTION FUNCTIONS AND SINGLE MOLECULE C.C.F'S AND A.C.F'S

Atom atom pair distribution functions (p.d.f.'s) were computed over about 5000 time steps. The oxygen to oxygen (O O) p.d.f. is compared in table 2 with equivalent results from Rahman and Stillinger [2] ; from the two

TABLE 2

Oxygen Oxygen P.d.f.'s

T/K	Potential	R_1(Å)	R_2(Å)	R_3(Å)	$r(M_1)$	M_1	$r(M_2)$	M_2
314	ST2 [2]	2.63	3.21	4.31	2.86	3.06	4.74	1.0
300	Clementi [3]				2.80	2.45	4.00	1.0
300	This work	2.73	3.70	5.25	3.10	2.18	5.66	1.2
323	Experimental[2,3]	2.64	3.31	4.21	2.85	2.28	4.75	1.1

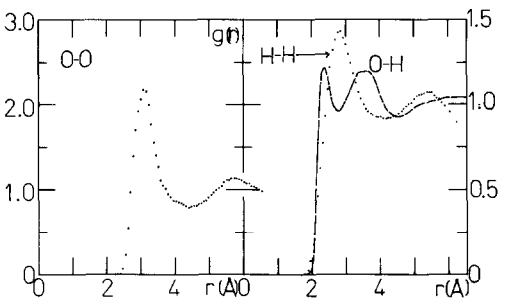

Fig. 5. Atom-atom p.d.f.'s from the computer simulation.
Ordinate normalised p.d.f. Abscissa Å

body Monte Carlo simulation of Clementi et al. [3] and with experimental results [2,3]. The notation in table (2) is the original one used by Stillinger and Rahman [2]. In fig. (5) we illustrate all three atom atom p.d.f.'s for water from our simulation. It is seen that the potential used in this work has strengths and weaknesses. In table (2) the first peak of the experimental (O O) p.d.f. at 323 K is reproduced better in intensity than ST2 but the maximum of the second peak occurs too far from the origin. In this respect ($r(m_2)$) Clementi et al. [3] seem to be too near the origin by about the same distance. The experimental second peak position seems to be uncertain to about ± 0.5 Å. The (H O) and (H H) p.d.f.'s of this work (fig. (5)) are broadly similar to detail to the original ST2 but again the individual peaks are much less sharply defined, the troughs much shallower. Our results seem therefore to be in much better agreement with the experimental data as regards the intensity of the first peak, but the overall agreement with

the second peak of the (O O) p.d.f. is less satisfactory than that obtained by Clementi et al. [3,5]

SINGLE MOLECULE TIME CORRELATION FUNCTIONS

Using the rotating frame theory of molecular diffusion significant progress has been achieved recently [7,8] in understanding the role of single molecule c.c.f.'s in condensed molecular matter. The existence of c.c.f.'s in the moving frame of reference [25] (1,2,3) of the principal molecular moments of inertia has been confirmed in this work,showing that it is not useful to restrict the analytical treatment of diffusion in liquid water to "pure rotation" or "pure translation". Further evidence for pronounced and intricate cross correlation between the rotational and translational dynamics of the water molecule is presented in this section with respect to the a.c.f.'s of the classical Coriolis, centripetal, and non-linear accelerations of H_2O both in frame (1,2,3) and directly in the laboratory frame (x,y,z). There seems little doubt that there exist similar time correlations between vibrational modes of the (H O) intra and inter molecular bonds and the rotation and translation of the whole molecule. All these c.c.f.'s contribute indirectly to spectral features such as those in the far and mid infra-red, i.e. the high frequency parts of the well known Debye type dielectric loss curve in water.

TIME AUTOCORRELATION FUNCTIONS

It is possible to extract the whole range of a.c.f.'s from our simulation starting with the direct comparison in figs. (6) and following with the a.c.f.'s given by Stillinger and Rahman [2] and by Clementi and co workers. [3,5] The latter provide a.c.f.'s of the linear centre of mass molecular velocity ($\underset{\sim}{v}$) and the molecular angular velocity ($\underset{\sim}{\omega}$) in the moving frame of reference (1,2,3). The former illustrate the a.c.f.'s of $\underset{\sim}{v}$ in the laboratory frame (x,y,z).

In fig. (6) the a.c.f. of $\underset{\sim}{\omega}$ from this simulation is illustrated in both frames together with the second order a.c.f. $\langle\underset{\sim}{\omega}(t).\underset{\sim}{\omega}(t)\underset{\sim}{\omega}(o).\omega(o)\rangle/\langle\omega^4\rangle$ in the laboratory. The three individual moving frame a.c.f. components seem to be slightly more oscillatory than those of Clementi et al. [3] but show the same kind of anisotropy in the angular motion of the $(H_2O)_1$ molecule. The laboratory frame a.c.f. $\langle\underset{\sim}{\omega}(t).\underset{\sim}{\omega}(o)\rangle/\langle\omega^2\rangle$ not shown by Clementi et al., is oscillatory on the picosecond time scale and so is the second order a.c.f.

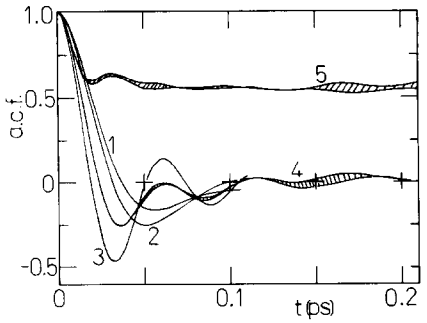

Fig. 6. Angular velocity a.c.f.s from the computer simulation.

1. $\langle\omega_1(t)\omega_1(o)\rangle/\langle\omega_1^2\rangle$; 2. $\langle\omega_2(t)\omega_2(o)\rangle/\langle\omega_2^2\rangle$;

3. $\langle\omega_3(t)\omega_3(o)\rangle/\langle\omega_3^2\rangle$; 4. $[\langle\underset{\sim}{\omega}(t).\underset{\sim}{\omega}(o)\rangle/\langle\omega^2\rangle]_{(x,y,z)}$;

5 $[\langle\omega(t).\underset{\sim}{\omega}(t)\underset{\sim}{\omega}(o).\underset{\sim}{\omega}(o)\rangle/\langle\omega^4\rangle]_{(x,y,z)}$.

defined already. In the context of the angular motion of the $(H_2O)_1$ molecule in liquid water, fig. (7) shows that the first and second angular momentum a.c.f.'s are not the same as the equivalent angular velocity a.c.f.'s because of the anisotropy of the moment of inertia tensor in H_2O.

Fig. (8) is the equivalent of fig. (6) for $\underset{\sim}{v}$. The laboratory frame a.c.f.

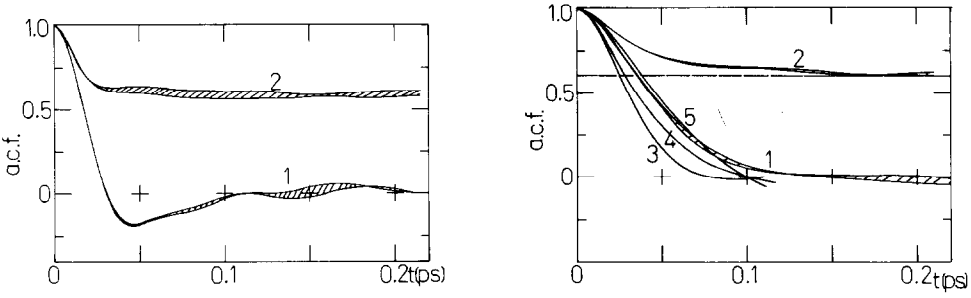

Fig. 7. Angular momentum a.c.f.'s in the laboratory frame from the computer simulation.

1. $\langle J(t).J(o)\rangle/\langle J^2\rangle$; 2. $\langle\underset{\sim}{J}(t).\underset{\sim}{J}(t)\underset{\sim}{J}(o).\underset{\sim}{J}(o)\rangle/\langle J^4\rangle$.

where $\underset{\sim}{J}$ is the resultant laboratory frame angular momentum of the H_2O molecule.

Fig. 8. Linear centre of mass velocity a.c.f.'s

1. $(\langle\underset{\sim}{v}(t).\underset{\sim}{v}(o)\rangle/\langle v^2\rangle)_{x,y,z}$ 2. $(\langle\underset{\sim}{v}(t).\underset{\sim}{v}(t)\underset{\sim}{v}(o).\underset{\sim}{v}(o)\rangle/\langle v^4\rangle)_{x,y,z}$

3. $\langle v_1(t)v_1(o)\rangle/\langle v_1^2\rangle$ 4. $\langle v_2(t)v_2(o)\rangle/\langle v_2^2\rangle$

5. $\langle v_3(t)v_3(o)\rangle/\langle v_3^2\rangle$.

seems to be less oscillatory than the equivalent from Stillinger and Rahman [2] but the moving frame a.c.f. components in fig. (8) are similar to those obtained from Clementi et al. [3] with full consideration of multi body interactions with their ab initio potential energy surface. The second order a.c.f. $\langle \underset{\sim}{v}(t).\underset{\sim}{v}(t)\underset{\sim}{v}(o).\underset{\sim}{v}(o)\rangle/\langle v^4$ in the laboratory frame. The three individual moving frame a.c.f. components seem to be slightly more oscillatory than those of Clementi et al. [3] but show the same kind of anisotropy in the angular motion of the $(H_2O)_1$ molecule. The laboratory frame a.c.f. $\langle \underset{\sim}{\omega}(t).\underset{\sim}{\omega}(o)\rangle/\langle\omega^2\rangle$ not shown by Clementi et al., is oscillatory on the picosecond time scale and so is the second order a.c.f. defined already. In the context of the angular motion of the $(H_2O)_1$ molecule in liquid water, fig. (7) shows that the first and second angular momentum a.c.f.'s are not the same as the equivalent angular velocity a.c.f.'s because of the anisotropy of the moment of inertia tensor in H_2O.

Fig. (8) is the equivalent of fig. (6) for $\underset{\sim}{v}$. The laboratory frame a.c.f. seems to be less oscillatory than the equivalent from Stillinger and Rahman [2] but the moving frame a.c.f. components in fig. (8) are similar to those obtained from Clementi et al. [3] with full consideration of multi body interactions with their ab initio potential energy surface. The second order a.c.f. $\langle \underset{\sim}{v}(t).\underset{\sim}{v}(t)\underset{\sim}{v}(o).\underset{\sim}{v}(o)\rangle/v^4$ of the laboratory frame (x,y,z) reaches the theoretical limit of 2/3 for equilibrium Gaussian statistics, but there is an immediate non Gaussian behaviour at around 0.1 ps from the time origin. It is known that [26,27] this provides information on the role of the effective potential well in the theory of non linear non equilibrium statistical mechanics. [28] The anisotropy of the moving frame component a.c.f.'s of $\underset{\sim}{v}$ in fig. (8) is corroborated in the work of Clementi et al. and is also known experimentally. [3]

The reorientational dynamics of the $(H_2O)_1$ molecule are of prime interest for far infra-red power absorption (fig. (4)) and for dielectric relaxation. Fig. (9) summarises the first order reorientational properties of $(H_2O)_1$ in liquid water through the laboratory frame a.c.f.'s of $\underset{\sim}{e}_1$, $\underset{\sim}{e}_2$ and $\underset{\sim}{e}_3$ and their time derivatives $\dot{\underset{\sim}{e}}_1$, $\dot{\underset{\sim}{e}}_2$ and $\dot{\underset{\sim}{e}}_3$. The unit vectors $\underset{\sim}{e}_1$, $\underset{\sim}{e}_2$ and $\underset{\sim}{e}_3$ define the principal molecular moment of inertia axes 1,2 and 2 (fig. (1)) and the molecular dipole moment μ is in axis 1 in this notation. The a.c.f. $\langle \underset{\sim}{\mu}(t).\underset{\sim}{\mu}(o)\rangle$ is indirectly observable by dielectric relaxation with the aid of macro to micro correlation theorems, [10] and as we have noted already, $\langle \dot{\underset{\sim}{\mu}}(t).\dot{\underset{\sim}{\mu}}(o)\rangle$, the rotational velocity a.c.f., is indirectly related to the far infra red power absorption coefficient (figs. (3) and (4)).

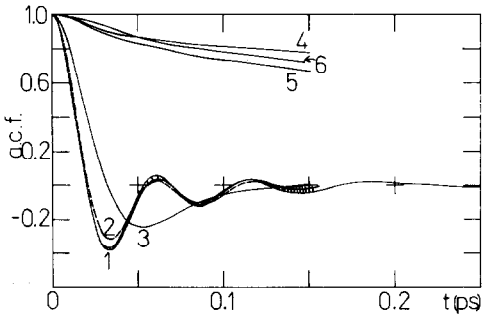

Fig. 9. Laboratory frame orientational and rotational velocity a.c.f.'s

1. $\langle \dot{e}_{\underset{\sim}{1}}(t).\dot{e}_{\underset{\sim}{1}}(o)\rangle/\langle \dot{e}_1^2\rangle$
2. $\langle \dot{e}_{\underset{\sim}{2}}(t).\dot{e}_{\underset{\sim}{2}}(o)\rangle/\langle \dot{e}_2^2\rangle$
3. $\langle \dot{e}_{\underset{\sim}{3}}(t).\dot{e}_{\underset{\sim}{3}}(o)\rangle/\langle \dot{e}_3^2\rangle$
4. $\langle e_{\underset{\sim}{1}}(t).e_{\underset{\sim}{1}}(o)\rangle/\langle e_1^2\rangle$
5. $\langle e_{\underset{\sim}{2}}(t).e_{\underset{\sim}{2}}(o)\rangle/\langle e_2^2(o)\rangle$
6. $\langle e_{\underset{\sim}{3}}(t).e_{\underset{\sim}{3}}(o)\rangle/\langle e_3^2\rangle$

The well known minimum [2,5] in the orientation a.c.f. $\langle \underset{\sim}{\mu}(t).\underset{\sim}{\mu}(o)\rangle$ is observable in curve (4) of fig. (9) at about 0.05 ps, but seems to be slightly shallower than in the original work of Rahman and Stillinger [2] or in the work of Lie and Clementi [5] using a fully ab initio interaction potential. Nevertheless the position is exactly the same (0.05 ps) and fig. (9) clearly shows that this feature in the orientational a.c.f. corresponds to the first minimum of the oscillatory rotational velocity a.c.f. $\langle \dot{\underset{\sim}{\mu}}(t).\dot{\underset{\sim}{\mu}}(o)\rangle$. Finally, fig. (9) shows clearly that the reorientational diffusion of the $(H_2O)_1$ molecule in liquid water is markedly anisotropic and this should be observable experimentally with, for example, N.M.R. relaxation [10] via the equivalent second order orientational a.c.f.'s. We have insufficient computer power to draw out $\langle \underset{\sim}{\mu}(t).\underset{\sim}{\mu}(o)\rangle$ further than shown in fig. (9) but the decay of this a.c.f. is in line with the results obtained by Lie and Clementi [5] with a fully ab initio inter molecular potential energy surface on the I.B.M. L.C.A.P. system.

INTER DEPENDENCE OF $(H_2O)_1$ ROTATION AND TRANSLATION

Progress has been made recently in this area by using a rotating frame of reference [8,29] to link the rotational and translational Langevin equations for the three dimensional diffusion of the asymmetric top molecule. The angular velocity of the rotating frame for each molecule in the ensemble is $\underset{\sim}{\omega}$, the molecular angular velocity, and its origin is always at that of the laboratory

frame itself. This provides two advantages over the conventional theory of diffusion [10] :

i) the need for friction cross-coefficients to link the rotational and translational Langevin equations is removed;

ii) the existence of new acceleration terms involving $\underset{\sim}{v}$ and the position $\underset{\sim}{r}$ of the molecular centre of mass becomes clear.

These results are valid for molecular diffusion in condensed molecular matter. The theory predicts the existence of three new types of molecular acceleration [29,30] in the laboratory frame and also in the moving frame defined by the principal molecular moments of inertia. These are:

1) the molecular Coriolis acceleration $2\underset{\sim}{\omega}(t) \times \underset{\sim}{v}(t)$;

2) the molecular centripetal acceleration, $\underset{\sim}{\omega}(t) \times (\underset{\sim}{\omega}(t) \times \underset{\sim}{r}(t))$;

3) the non-uniform acceleration $\dot{\underset{\sim}{\omega}}(t) \times \underset{\sim}{r}(t)$.

It follows that there exist in both frames of reference a.c.f.'s of these forces and also numerous c.c.f.'s among them. These are illustrated for water in fig. (10) and have been computed using the methods of section 1. These results prove, inter alia, the validity of the new rotating frame theory [8] and also the existence of fundamental, classical, molecular accelerations

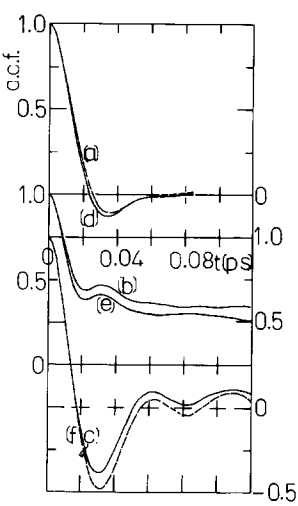

Fig. 10. a) The a.c.f of the H_2O classical Coriolis acceleration, frame (x,y,z) normalised to unity at t=0. b) A.c.f. of the classical centripetal acceleration, (x,y,z). c) A.c.f. of the classical non-uniform acceleration, (x,y,z) d) As for a) frame (1,2,3).
e) As for b) frame (1,2,3). f) As for c) frame (1,2,3).

involving the rotational and translational motions of $(H_2O)_1$ simultaneously. This destroys the physical validity of historical concepts of "purely rotational" and "purely translational" diffusion. [10] Furthermore the computer simulation method used to produce them has been tested thoroughly in this paper against experimental data and other simulations [3,5] of liquid water. Therefore fig. (10) is a good (classical) representation of the a.c.f. as it might appear in reality.

SINGLE MOLECULE CROSS CORRELATION FUNCTIONS

The new rotating frame theory also predicts [8,30] the existence in the principal moment of inertia frame (1,2,3) of numerous new c.c.f.'s between different vectors on the same molecule. The first moving frame c.c.f. was computed by Ryckaert et al. [25] in 1981 in frame (1,2,3):

$$C_1(t) = \frac{\langle \underset{\sim}{\omega}(t) \underset{\sim}{\chi}^T(o) \rangle}{\langle \omega^2 \rangle^{\frac{1}{2}} \langle v^2 \rangle^{\frac{1}{2}}} \qquad (3)$$

This tensor product describes [4,6,31] the statistical correlation between the diffusing molecule's centre of mass linear velocity and its own angular velocity a time t later.

Fig. (11) shows that the non vanishing off diagonal elements of $C_1(t)$ for liquid water. The hatched area denotes the difference between two

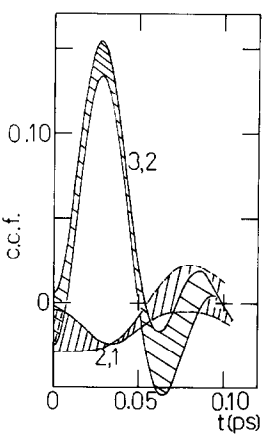

Fig. 11. Non-vanishing elements of $\langle \underset{\sim}{\omega}(t) \underset{\sim}{\chi}^T(o) \rangle$ in frame (1,2,3).

$$(i,j) \equiv \langle \omega_i(t) v_j(o) \rangle / (\langle \omega_i^2 \rangle^{\frac{1}{2}} \langle v_j^2 \rangle^{\frac{1}{2}})$$

segments each of about 1000 time steps and is a measure of the noise generated in the run by lack of computer power. The intensity at peak height of the normalised elements in fig. (11) shows the strength of this kind of first order cross correlation. The rotating frame diffusion theory provides a means of accounting for the existence of $C_1(t)$ and, furthermore, predicts the possible existence of numerous higher order single molecule c.c.f.'s.

About four hundred separate single molecule c.c.f.'s of this type have each been computed recently [30] for the asymmetric top dichloromethane. The symmetry pattern that emerged from this work is reported elsewhere. This work [30] shows the effect of destroying parity reversal invariance for the total hamiltonian with an external electric field ($+\underset{\sim}{E}$). The tensor c.c.f.'s computed for liquid water are

$$C_2(t) = \langle \underset{\sim}{\omega}(t) x \underset{\sim}{r}(t) \underset{\sim}{\omega}^T(o) \rangle / [\langle \omega^2 \rangle \langle r^2 \rangle^{\frac{1}{2}}] , \tag{4}$$

$$C_3(t) = \frac{\langle \underset{\sim}{\omega}(t) x (\underset{\sim}{\omega}(t) x \underset{\sim}{r}(t)) \ (\underset{\sim}{\omega}(o) x \underset{\sim}{r}(o))^T \rangle}{\langle \omega^2 \rangle \ \langle \omega^2 \rangle^{\frac{1}{2}} \langle r^2 \rangle} , \tag{5}$$

$$\underset{\sim}{C}_4 = \langle \underset{\sim}{v}(t) \ x \ \underset{\sim}{\omega}(t) \underset{\sim}{v}^T(o) \rangle / [\langle v^2 \rangle \langle \omega^2 \rangle^{\frac{1}{2}}], \tag{6}$$

$$\underset{\sim}{C}_5 = \langle \underset{\sim}{\omega}(t) \ x \ \underset{\sim}{v}(t) \underset{\sim}{\omega}^T(o) \rangle / [\langle \omega^2 \rangle \langle v^2 \rangle^{\frac{1}{2}}] \tag{7}$$

$$\underset{\sim}{C}_6 = \langle \underset{\sim}{r}(t) \ x \ \underset{\sim}{\omega}(t) \underset{\sim}{r}^T(o) \rangle / [\langle r^2 \rangle \langle \omega^2 \rangle^{\frac{1}{2}}]. \tag{8}$$

A number of the elements of c.c.f. tensors for liquid dichloromethane have also been individually computer simulated as reported elsewhere. [30] These all vanish in both frames for all E_z.

This illustrates the selection rules governing the existence of c.c.f.'s in molecular condensed matter. The group symmetry of the water molecule is the same as that of the dichloromethane molecule, i.e. C_{2v}. Therefore the overall symmetry pattern of the c.c.f.'s in frame (1,2,3) will be the same in both liquids. The details of time dependence in each c.c.f. will naturally be different because the intermolecular forces are different and the molecular inertia distribution in each molecule is responsible for the anisotropy in time dependence of the c.c.f. elements.

It is a major computational task [30] to investigate for liquid water the numerous c.c.f.'s which are symmetry allowed in frame (1,2,3). Some of these are illustrated in figs (12) to (15). It can be seen that moving frame diagonal elements exist of the type $\langle \underset{\sim}{A}(t) \ x \ \underset{\sim}{\omega}(t) \underset{\sim}{A}^T(o)$ where $\underset{\sim}{A} = \underset{\sim}{v}, \underset{\sim}{\omega} x \underset{\sim}{r}$ or $\underset{\sim}{r}$. There is a suggestion (above the noise in fig. (15)) that some of the off-diagonal elements in $\underset{\sim}{C}_5(t)$ may exist directly in the laboratory frame (x,y,z).

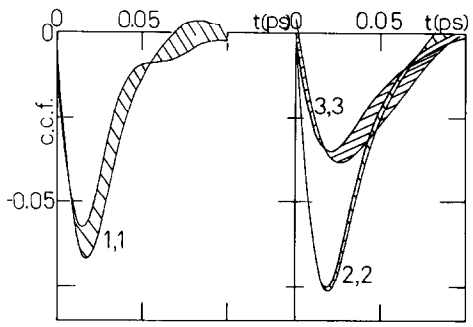

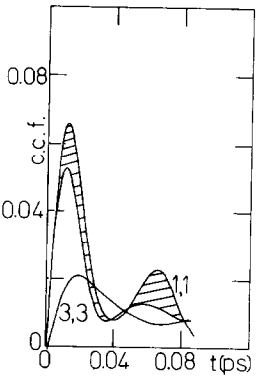

Fig. 12. The non-vanishing elements of $\langle \underset{\sim}{v}(t) \times \underset{\sim}{\omega}(t) \underset{\sim}{v}^{T}(o) \rangle$ in frame (1,2,3);

$$(i,i) = \frac{\langle (\underset{\sim}{v}(t) \times \underset{\sim}{\omega}(t))_i v_i(o) \rangle}{\langle v^2(o) \rangle \langle \omega^2(o) \rangle^{\frac{1}{2}}}$$

Fig. 13. As for fig. (12);

$$\frac{\langle \underset{\sim}{\omega}(t) \times (\underset{\sim}{\omega}(t) \times \underset{\sim}{r}(t)) (\underset{\sim}{\omega}(o) \times \underset{\sim}{r}(o))^{T} \rangle}{\langle \omega^2(o) \rangle \langle \omega^2(o) \rangle^{\frac{1}{2}} \langle r^2(o) \rangle}$$

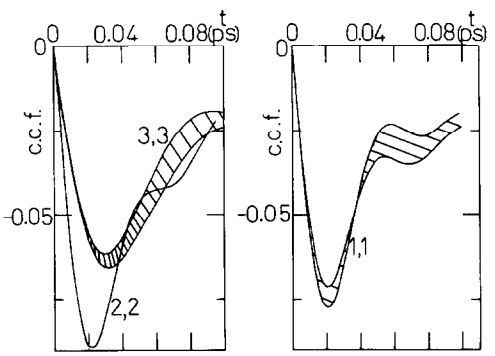

Fig. 14. As for fig. (12)

$$\frac{\langle \underset{\sim}{r}(t) \times \underset{\sim}{\omega}(t) \underset{\sim}{r}^{T}(o) \rangle}{\langle r^2(o) \rangle \langle \omega^2(o) \rangle^{\frac{1}{2}}}$$

These elements have been reported elsewhere [30] for CH_2Cl_2 where $\underset{\sim}{C}_5(t)$ (laboratory frame) is an antisymmetric tensor with vanishing diagonal elements. These c.c.f.'s are new diagonal dynamical properties of the molecular condensed state in general.

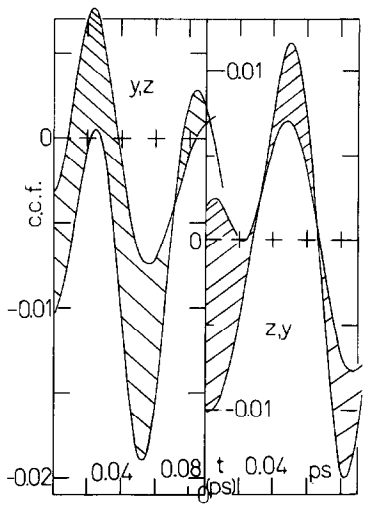

Fig. 15. Possible non-vanishing elements of $\langle \underset{\sim}{\omega}(t) \times \underset{\sim}{y}(t) \underset{\sim}{\omega}^{T}(o) \rangle$ in the laboratory frame (x,y,z). The elements illustrated here seem to exist above the computer noise generated by the results of three different segements of 1000 time steps each. Greater computer power is needed to cut down the noise.

GROUP THEORETICAL ANALYSIS OF MOVING FRAME C.C.F.'S

The existence of the c.c.f.'s in frame (1,2,3) can be predicted by group theory, provided that the sample is isotropic and that it is free from a parity breaking external field. The use of group theory in this way serves as a useful check on the computer simulation results and indeed confirms the validity of the m.d. methods used in this paper.

For example, $\underset{\sim}{C}_4(t)$ is reducible in frame (1,2,3) in an isotropic environment in frame (1,2,3) as nine elements, of which, A_1 is the only property which survives after averaging in the absence of anisotropy. For example, if the tensor is the outer product of two vectors (both polar or both axial) A_1 applies and refers for example to the triple product $\langle \underset{\sim}{y}(t) \times \underset{\sim}{\omega}(t) . \underset{\sim}{y}(o) \rangle$ which is a scalar. The A_2 case refers to a pseudo-scalar which might be the product of an axial and a polar vector. These products are only non zero on average for point groups which embrace optically active molecules. Consequently, $C_4(t)$ reduces to the renormalised triple product multiplied by the appropriate weighting tensor. This implies that the

(1,1) (2,2) and (3,3) elements of $C_4(t)$ exist in frame (1,2,3) and these are illustrated in the text of this paper. The group theory implies that all other elements of this tensor must vanish in frame (1,2,3) (the off diagonal elements) and all elements of frame (x,y,z). This is actually what is found in the simulation. At the time origin the triple product must vanish for all the molecules in the ensemble because two out of the three vectors in the product are equal. The application of group theory therefore shows that the computer simulation provides the elements which exist theoretically on the grounds of molecular symmetry in an isotropic environment.

ACKNOWLEDGEMENTS

The Nuffield Foundation and Leverhulme Trust are thanked for grants and the University of Wales for a Fellowship. The University of Pisa is thanked for the award of a travel grant and Professor E. Clementi for several preprints. IBM is thanked for a Visiting Professorship to MWE.

REFERENCES

1 M.D. Morse and S.A. Rice, J. Chem. Phys., 76 (1982) 650

2 F.H. Stillinger and A. Rahman, J. Chem. Phys., 60 (1974) 1545; ibid 55 (1973) 3336; 57 (1972) 1281; 61 (1974) 4973; 68 (1978) 666; These authors refer to experimental results, e.g. A.H. Narten and H.A. Levey, J. Chem. Phys., 55(5) (1971) 2263, which have been used in Table 2.

3 E. Clementi, G. Corongiu, J.H. Detrich, H. Kahnmohammadbaigi, S. Chin, L. Doningo, A. Laaksonen and M.N. Ngyuen, Physica, 131 B & C, (1974) 74

4 E. Kluk and M. Herman, in "Dynamical Processes in Condensed Matter", vol. 63 of "Advances in Chemical Physics", ed. M.W. Evans, series ed. I. Prigogine and S.A. Rice (Wiley Interscience, New York, 1985).

5 G.C. Lie and E. Clementi, "Molecular Dynamics Simulation of Liquid Water with an Ab Initio Flexible Water Water Interaction Potential" IBM DSD, KGN 36.

6 M.W. Evans, Phys. Rev. Letters 50 (1983) 371

7 M.W. Evans and G.J. Evans, Phys. Rev. Letters 55 (1985) 818

8 M.W. Evans, Phys. Rev. Letters 55 (1985) 1551; Phys. Rev., A. Rapid Comm. 33 (1986) 2193

9 See review in ref. (4) and also ref. (4) vol, 62, ed. M.W. Evans. P. Grigolini and G. Pastori Parravicini.

10 M.W. Evans, G.J. Evans, W.T. Coffey and P. Grigolini, "Molecular Dynamics" (Wiley Interscience, New York, 1982).

11 For a comprehensive review see D. Bertolini, M. Cassettari, M. Ferrario, P. Grigolini, and G. Salvetti in vol. 62 of ref (4), chapter VII.

12 E. Eliel, N.L. Allinger, S.J. Angyal and G.A. Morrison, in "Conformational Analysis", (Wiley, New York, 1965).

13 D. Fincham and D.M. Heyes, ref. (4), chapter (5).

14 M. Ferrario and M.W. Evans, Adv. Mol. Rel. Int. Proc. 22 (1982) 245.

15 A.I. Baise, Thesis, University of Wales, (1971).

16 J.K. Vij and F. Hufnagel, in ref. (4).

17 J.K. Vij, C.J. Reid and M.W. Evans, Mol. Phys., 50 (1983) 935; Chem. Phys. Letters 92, (1982) 528; A.E. Stanevich and N.G. Yaroslavskii, Opt. Spectrosc., 11, (1961) 276.

18 O.A. Simpson, B.L. Bean and S. Perkowitz, J. Opt. Soc. America, 69 (1980) 1723.

19 J.B. Hasted, S.K. Husain, F.A.M. Frescura and J.R. Birch, Chem. Phys. Letters 118 (1985) 622.

20 G.J. Evans, communication.

21 J.K. Vij, F. Hufnagel, M. Helker and C.J. Ried, Communication.

22 G.J. Evans, Unpublished work with Messrs. Nicolet Instruments Ltd.

23 M.W. Evans, J. Chem. Soc., Faraday Trans. II, in press (1986).

24 M.W. Evans, ibid. 72 (1976) 2138.

25 J.P. Ryckaert, A. Bellemans and G. Ciccotti, Mol. Phys., 44 (1981) 979.

26 See ref. (4), vol. 62.

27 Ref. (4), vol 63, chapter II.

28 J. Smythe, F. Moss and P.V.E. McClintock, Phys. Rev. Letters, 51 (1983) 1062.

29 M.R. Spiegel, "Vector Analysis", (Schaum, New York, 1958), p. 53

30 M.W. Evans, Phys. Rev. A 33 (1986) 1903.

31 M.W. Evans and G.J. Evans, Phys. Rev. A, in press, (July 1986).

32 M.W. Evans, Phys. Rev. A, in press, (September 1986).